7

A Novel Approach to Evaluate the Sensitivities of the Optical Fiber Evanescent Field Sensors

Xuye Zhuang[1], Pinghua Li[2] and Jun Yao[1]
[1]*State Key Laboratory of Optical Technologies for Microfabrication, Institute of Optics and Electronics, Chinese Academy of Sciences*
[2]*Department of Electronic Information Technology, Sichuan Modern Vocational College*
China

1. Introduction

Optical fiber evanescent field sensors(OFEFS) are playing more and more important roles in detecting chemical, bacilli, toxin, and environmental pollutants for their high efficiency, good accuracy, low cost, and convenience (Maria et al., 2007; Wolfbeis, 2006; Angela et al., 2007). In general, these sensors exploit the interactions between evanescent field of the sensing fibers and the surrounding analyte under investigation. Concentrations of analyte can be related to the power attenuation caused by these interactions, and the more energy interacted with the analyte, the higher the sensitivities of the sensors. In order to expose the evanescent filed of the fiber to the analyte, the fiber cladding is often removed and the fiber core is surrounded by the detecting material. To make clear the operation principle of the evanescent field interacting with the analyte and to estimate the sensitivity according to this principle are extremely important to the sensor's designers. This field has attracted a lot of research groups extraordinarily and been widely discussed both based on geometric optics and optical waveguide theory (Yu et al., 2006; Messica et al.,1996; Gupta & Singh, 1994; Guo & Albin, 2006). However a big difference between the theoretical and experimental values is often observed especially when the sensor's absorbency is low (Payne & Hale, 1993; Wu et al., 2007; Deng, et al., 2006).

In this chapter, a thoroughly theoretical study of the OFEFS is presented. The reason why the sensor's absorbency, A, shows nonlinear increase with the sensing fiber's length, l, is given and analyzed. Also, a new method to estimate the sensitivity of the sensor is proposed and confirmed with experimental results, which shows a good agreement with the experimental results and is more accurate than the methods used before. The fabrication technologies of the sensing fibers are introduced. The practical importance of this study lies in helping for understanding, design and construction of optical fiber evanescent field sensors.

This chapter is organized as follows. In section 2, the theory basis of the optical fiber evanescent field sensor is introduced and analyzed. The nonlinear relationship between A and l is discussed theoretically. The new method to estimate the sensitivity of the sensor is proposed in section 2.3. The fabrication method of the sensing fiber with acicular

encapsulation is described in section 3. Also, the experiments used to confirm the new method and the nonlinear relationship between A and l are implemented and the results are analyzed. Finally, the contents of the chapter are summarized briefly in section 4.

2. Theory analysis of optical fiber evanescent field sensors

2.1 Evanescent field of the optical fiber

Optical fiber consists of a cylindrical core and a surrounding cladding, both made of silica, as illustrated in Fig. 1. The core is generally doped with germanium to make its refractive index n_{co} slightly higher than the refractive index of the cladding n_{cl} .

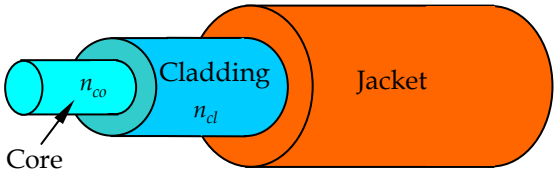

Fig. 1. The structure of step-index fiber

If a ray is launched into the fiber and its propagation angle θ_2 is greater than the critical angle θ_c , which is defined by the Eq.(1), the light will propagate along the fiber by total internal reflection (TIR).

$$\theta_c = \arcsin(n_{cl} / n_{co}) \tag{1}$$

Fig. 2 shows a hypothetical ray of light propagating along the fiber. n_0 is the refractive index of the air. θ_0 is the incident angle of the light at the core-air interface, which must obey the relationship described in Eq.(2) in order that the incident light can propagate along the fiber by TIR.

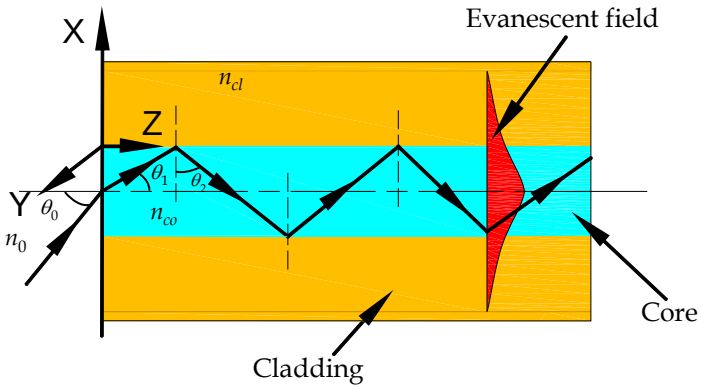

Fig. 2. The schematic of the light rays transmitting in the evanescent field sensing fiber

$$\sin\theta_0 < \frac{1}{n_0}(n_{co}^2 - n_{cl}^2)^{\frac{1}{2}} \tag{2}$$

θ_m is the maximum value of θ_0 and defined by Eq.(3).

$$n_0 \sin\theta_m = (n_1^2 - n_2^2)^{\frac{1}{2}} = NA \tag{3}$$

If the incident angle of a ray is smaller than θ_m, that ray of light will propagate along the fiber by TIR. *NA* is the numerical aperture of the fiber, which is a dimensionless number that characterizes the range of the incident angles over which the light can transmit by TIR in the fiber.

Though the light propagates along the fiber by TIR, there is energy penetrating into the cladding. The electric field amplitude of this field decays exponentially from the core-cladding interface and is described as Eq.(4).

$$E_x = E_0 e^{-x/d_p} \tag{4}$$

Where x is the distance from the core-cladding interface, E_0 is the electric field magnitude of the field at the interface, and d_p represents the penetration depth, which is the distance where the evanescent field decreases to $1/e$ of its value at the core-cladding interface and is mathematically given by (Zhuang et al., 2009a)

$$d_p = \frac{\lambda_0}{2\pi(n_{co}{}^2 \sin^2\theta_2 - n_{cl}{}^2)^{1/2}} \tag{5}$$

where λ_0 is the wavelength of the light source in the vacuum. Because of the non-absorbing cladding, no energy loss is measured in the fiber. When an absorbing media substitutes for the cladding, the intensity of the evanescent field is attenuated and the total transmitted energy in the fiber is reduced. These losses are caused by the interactions between the analyte and the evanescent field. A bigger d_p indicates a wider scope covered by the field, more chances of the energy interacts with the analyte, a bigger loss of the energy and a higher sensitivity of the sensor.

2.2 Mathematical mode of the optical fiber evanescent field sensor

The structure of the optical fiber evanescent field sensor is shown in Fig.3. One portion of the fiber's cladding is removed, and its core is exposed to the analyte directly. So the energy of the evanescent field can interact with the analyte, and the concentrations of the analyte can be detected by measuring the loss of the output power of the sensing fiber. The extent of the energy loss can be marked by the absorbency of the sensor, *A*, which is described as follows.

$$A = -\log_{10}\left(\frac{P_{out}}{P_{in}}\right) \tag{6}$$

where P_{out} and P_{in} are the output power of the optical fiber evanescent field sensors with and without an absorptive analyte for sensing. When detecting the same sample with the

same concentrations, the bigger the value, the more sensitive the sensor. It shows clearly in Eq.6 that the sensitivity of OFEFS can also be evaluated by the value of P_{out} / P_{in}. When detecting the same sample, the smaller the value, the higher the sensor's sensitivity.

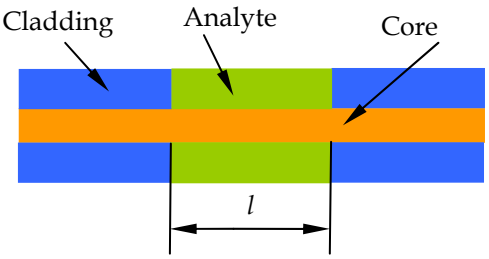

Fig. 3. Schematic diagram of the optical fiber evanescent field sensor

According to Beer's law, P_{out} is expressed as (Wu et al., 2007)

$$P_{out} = \sum_{j=1}^{N} r_j P_{in} \exp(-\alpha \eta_j l), \tag{7}$$

Subscript j stands for the jth mode optical waveguide transmitting in the sensing fiber. Hence, r_j is the fraction of the optical power carried by the jth mode in the sensor. When using incoherent light source, the energy carried by each mode transmitting in the sensing fiber is almost the same (Gloge, (1971). Also, after a long length of transmitting, the energy of each mode is almost equal through energy couples between different modes in the fiber (Zhuang et al., 2009a). So Eq.(8) can be modified as (Payne & Hale, 1993),

$$P_{out} = \frac{P_{in}}{N} \sum_{j=1}^{N} \exp(-\alpha \eta_j l) \tag{8}$$

where l is the length of the sensing fiber whose cladding is removed, α is the absorption coefficient of the analyte and is expressed as

$$\alpha = \frac{\varepsilon c}{\log_{10} e} \tag{9}$$

where ε and c are molar absorption coefficient and concentration of the analyte, respectively.

η is the fraction of power transmitting in the fiber cladding that carried by evanescent field of the sensor and is depicted as,

$$\eta = \frac{P_{cl}}{P_{cl} + P_{co}} \tag{10}$$

where P_{co} is the energy transmitting in the core; P_{cl} is the energy transmitting in the cladding in the form of evanescent field, which is the only energy interacted with the analyte. η_j is the energy fraction of the jth mode transmitting in the cladding. η can be calculated using Eq.(11).

$$\eta = 1 - \frac{P_{co}}{P_{cl} + P_{co}} = 1 - \frac{\int_0^a \int_0^{2\pi} R_e(\vec{e} \times \vec{h}^*)\vec{l}_z r dr d\theta}{\int_0^\infty \int_0^{2\pi} R_e(\vec{e} \times \vec{h}^*)\vec{l}_z r dr d\theta} \tag{11}$$

The integral part of Eq.(11) is the Poyning Vector Integral in cylindrical coordinates. The vector $\vec{l}_z$ indicates that the Z axis of the coordinate is along the fiber's axis. The particular explanations of each parameter used in Eq.(11) are listed in the reference (Gloge, 1971).

For multimode sensing fibers, η_j can be calculated using Eq.(12).

$$\eta_j = {}^{j}\!\Big/\!_{N(2N-2j)^{0.5}} \tag{12}$$

where N is the number of the modes supported by the fiber and defined by

$$N = {}^{4\times V^2}\!\Big/\!_{\pi^2} \tag{13}$$

V is the normalized frequency of the fiber and expressed as

$$V = \frac{2\pi a}{\lambda}(n_{co}^2 - n_{cl}^2)^{1/2} \tag{14}$$

where a is the radius of the core, λ is the wavelength of the light. As to less-mode or single mode optical fibers, η of different modes should be calculated carefully based on optical waveguide theory (Zhuang, 2009b).

2.3 Nonlinear relationship between absorbency and the length of the sensing fiber

From Eq.(6) and Eq.(8), we can obtain Eq.(15) which describes the absorbency of the sensing fibers.

$$A = -\log_{10}\left(\frac{\alpha l}{N}\sum_{j=1}^{N}\exp(-\eta_j)\right) \tag{15}$$

The sensitivity of the optical fiber evanescent field sensors, M, is defined as the instantaneous change of the sensors' absorbency relative to the analyte.

$$M = dA / dC \tag{16}$$

dA is the sensitivity of the photoelectric detector, which is the least variance of the absorbency the equipment can distinguish. According to Eq.(15) and dA, the lowest concentrations of the analyte to be detected can be approximately estimated.

In experiments, the actual sensitivity of the sensor can be obtained by Eq.(17).

$$M' = {}^{\Delta A}\!\Big/\!_{\Delta C} \tag{17}$$

where ΔA is the difference of the sensors' absorbency obtained from two different detections, ΔC is the difference of the analytes' concentrations.

From Eq.(15) and Eq.(16), it is found the absorbency A and the sensitivity M of the sensor linearly increase with l. However, non-linear dependence of A and M on the l is often observed in experimental tests (Zhuang, 2009a, 2009b). So the equations listed above should be modified to obtain a more accurate simulation results.

It shows clearly in Eq.(5) that d_p is decided by the parameters λ, n_{co}, n_{cl} and the propagation angle θ_2 of the ray. As the evanescent field energy transmitting along the fiber, none of those parameters change. So the value of d_p keeps unchanged during the process. Because of the interactions between the evanescent field and the analyte, the amplitude of the field decreases quickly which is shown clearly in Fig.4. The portion of the energy transmitting in the cladding is defined by Eq.(11), which indicates the amplitude of the evanescent field of the sensing fiber. For multimode fibers, η_j is given approximately by Eq.(12), which is the function of N. N is decided by the normalized frequency V of the sensing fiber. As expressed in Eq.(14), V is determined by the characters of the sensing fiber, the wavelength of the light source and the analyte's refractive index. After an experiment system is set up, V and N are determined, hence η_j is determined.

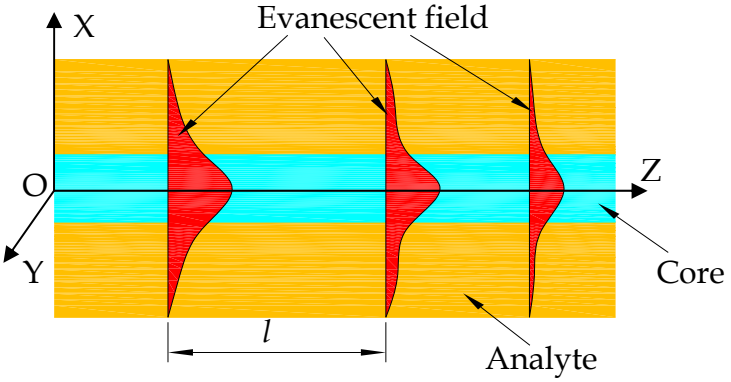

Fig. 4. Schematic of the evanescent field energy distribution along the sensing fiber

So η_j keeps constant along the sensing fiber's axis. As l grows, the evanescent field energy carried by the sensing fiber of unit length, which interacts with the analyte, decreases. That is to say the contribution per unit length of the sensing fiber to A decreases as l increased. So the linear relationship between A, M and L does not exist.

Consider a sensing fiber whose refractive index of the core is 1.4682 and the refractive index of the detecting material is 1.3334. The wavelength of the light source is 632.8nm, the sensing fiber is 14mm in length, 8μm in diameter, and its η_{120} and η_{200} are 0.0643 and 0.1104, respectively. Assume the energy carried by these two modes is both 1W, and the energy carried by the evanescent field is totally absorbed by the analyte. The calculated results of P_{cl} on different locations of the sensing fiber are shown in Fig.5. For η_{200}, the ratio of P_{cl} on the end of the sensing fiber to that on the beginning is just 19.47%, and it is 39.50%

for η_{120}. As l grows, the value of P_{cl} tends to be small. P_{cl} decreases much faster, when the order of the waveguide is higher. It indicates that the contribution per unit length of the sensing fiber to A becomes small as l grows, especially the ones close to the end of the sensing fiber. This is the essential reason why A does not increase linearly with l.

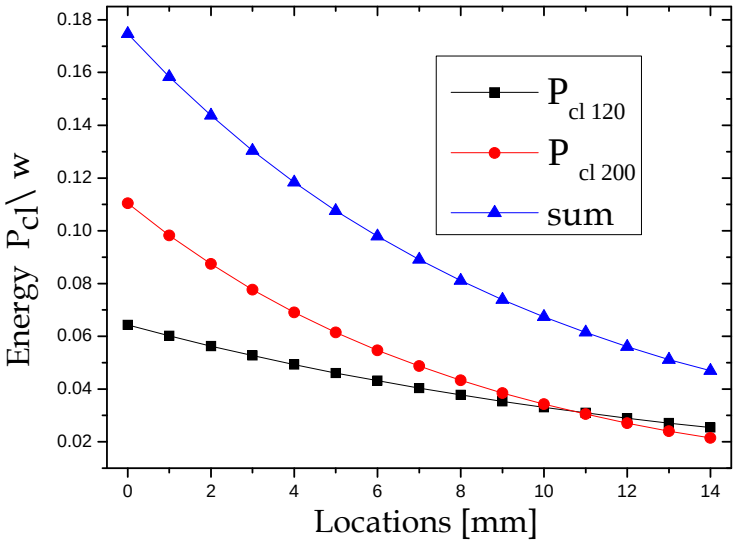

Fig. 5. P_{cl} on different locations of the sensing fiber

2.4 New method to estimate the sensitivity of the OFEFS

Considered that only P_{cl} interacts with the analyte and η is constant along the fiber axis, a new method to estimate the output power of OFEFS is proposed. In this method, the sensing fiber is evenly divided into n fractions with each part to be Δl in length as shown in Fig.6. As P_{cl} transporting along the sensing fiber, it is attenuating following Beer's law. Because η is constant along the whole sensing fiber, there is power replenishment to P_{cl} from the fiber core simultaneously. For each fraction, Δl is very small, so it can be assumed that the energy replenishment occurred at the end of Δl. The total energy left will be redistributed according to η at the beginning of the next Δl. The process repeats until the calculations on all the fractions have finished. As n trends to be infinite, the calculated result trends to be the real value. In this way the two most important factors, that is only the cladding power interacts with the analyte and η is constant along the fiber, are embodied significantly.

Now consider the power transmitting in the jth mode between the kth and the $(k+1)th$ parts of the sensing fiber. $P_{clj(k)}$ is the initial power transmitting in the cladding of the fiber of the kth Δl, and $P_{coj(k)}$ is the initial power in the core. $P'_{clj(k)}$ is the residual energy of $P_{clj(k)}$ after passing Δl. According to Beer's law

$$P'_{clj(k)} = P_{clj(k)} \exp(-\alpha \Delta l) = (r_j P_{in} \eta_j)_k \exp(-\alpha \Delta l) \tag{18}$$

Where $r_j P_{in} \eta_j$ means the power flowing in the cladding i.e. the power interacts with the analyte, and the subscript k means the kth Δl, hence $P_{clj(k)}$ stands for the cladding power in the kth Δl. Here η does not work as the index of the EXP function as in Eq.(8) but it is multiplied by $r_j P_{in}$ to form the power that interacts with the analyte. At the next Δl, the cladding power $P_{clj(k+1)} = \eta_j (P'_{clj(k)} + P_{coj(k)})$ is redistributed according to Eq. (10). Then the next calculation cycle begins.

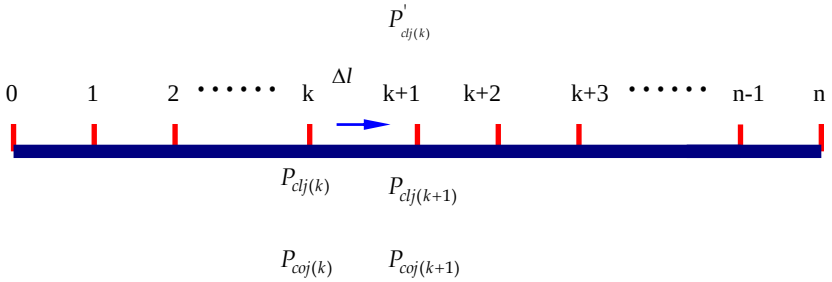

Fig. 6. Schematic diagram of the sensing fiber divided into n parts and the energy distribution

The absorbed energy $\Delta P_{clj(k)}$ caused by the analyte can be written by

$$\Delta P_{clj(k)} = P'_{clj(k)} - P_{clj(k)} = (\exp(-\alpha \Delta l) - 1) P_{clj(k)} \tag{19}$$

When $n \to \infty$, $\Delta P_{clj(k)} \to dP_{clj}$ and $\Delta l \to dl$, Eq. (19) becomes

$$\frac{dP_{clj}}{P_{clj}} = \exp(-\alpha dl) - 1 \tag{20}$$

Together with the initial condition, Eq.(20) and Eq.(10) form the mathematical model of OFEFS.

$$\begin{cases} \dfrac{dP_{clj}}{P_{clj}} = \exp(-\alpha dl) - 1 \\ \dfrac{P_{clj}}{P_{clj} + P_{coj}} = \eta_j \\ P_{clj(0)} + P_{coj(0)} = r_j P_{in} \end{cases} \tag{21}$$

Where P_{in} is the initial input power of the OFEFS. $P_{clj(0)}$ and $P_{coj(0)}$ are the initial values of P_{clj} and P_{coj}, respectively.

It is difficult to get an analytic solution of Eq.(21), but more convenient to solve it by numerical integration. Here we prefer to solve this question using recursion. The output power of the sensor after passing the whole sensing fiber can be expressed as

$$P_{out} = \frac{\sum_{j=1}^{N} P_{totj} - \sum_{j=1}^{N}\sum_{k=0}^{n} \Delta P_{clj(k)}}{\sum_{j=1}^{N} P_{totj}} P_{in} \tag{22}$$

where $P_{totj} = r_j P_{in}$ is the initial energy of the jth mode.

In order to facilitate calculation and obtain an estimated value of good accuracy, the convergence condition of Eq.(22) is set as

$$\begin{cases} \dfrac{(P_{out}/P_{in})_{n1} - (P_{out}/P_{in})_{n2}}{(P_{out}/P_{in})_{n1}} < 0.1\% \\ n_2 - n_1 > 1000 \end{cases} \tag{23}$$

where n_1 and n_2 are the iterative times of the recursion.

3. Experiment

3.1 Preparation of the sensing fiber

Optical fiber evanescent field sensors with acicular encapsulation are fabricated using MEMS silicon photolithography technology and silica wet-etching technology. This type of OFEFS is small, consuming little reagent, suffering from less deformation during the detection process and protecting the sensors from pollution. The sensors' sample cell consists of a cap and a bottom. The characters of the cap and the bottom are illustrated in Fig. 7.

The sizes of the cap and the bottom are both 1mm×20mm. There are two holes fabricated in the cap, which are the channels for the sample flow in and the waster drain out. The fiber slit in the bottom is used to fix the sensing fiber, which will facilitate the process of encapsulation greatly. The slit is 2.5mm in length, 250μm in width and 150μm in depth. The work of the cone that manufactured in the bottom is to guide the sample/de-ionized water into or out of the sample pool. The island stand in the sample pool is used to support the sensing fiber. The function of the slit decorated in the island is to fix the sensing fiber, which can avoid the sensing fiber from shaking. The slit is 140μm in width and 100μm in depth. The slit is 50μm shallower than the fiber slit. The fiber with cladding is thicker than the fiber whose cladding is removed. If these slits are made with the same depth, the sensing fiber will warp, the repeatability of the sensor will be poor and the results will be distorted. So using slits with different depth to support different parts of the fiber can help the sensing fiber keep straight in the sample pool. Sample pool is the place where the analyte interacts with the evanescent field. The width of the sample pool is 200μm, and 150μm in depth. The length of the pool can be chosen discretionary according to experimental requirements. When the length of the pool is 7mm, the total reagent the sensor consumed is only 0.21μl. Both the cap and the bottom are fabricated based on MEMS technologies.

In order to obtain high sensitivities, the radius of the sensing fiber is usually very small, such as 4μm. So the strength of the sensing fiber is weak, and the sensing fiber is fragile and

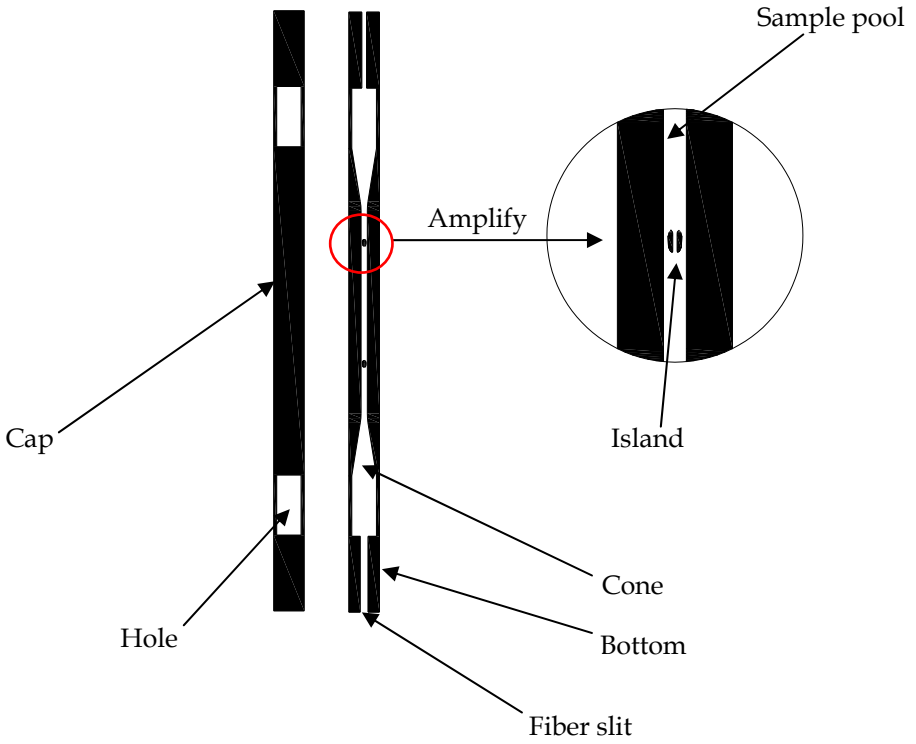

Fig. 7. The structure of the cap and the bottom

easy to break. In order to solve this problem, the fiber is fixed to the bottom first. Then, the cap is bound to the bottom to form the sensor's cell using glue. The construction of the cell is illustrated in Fig.8.

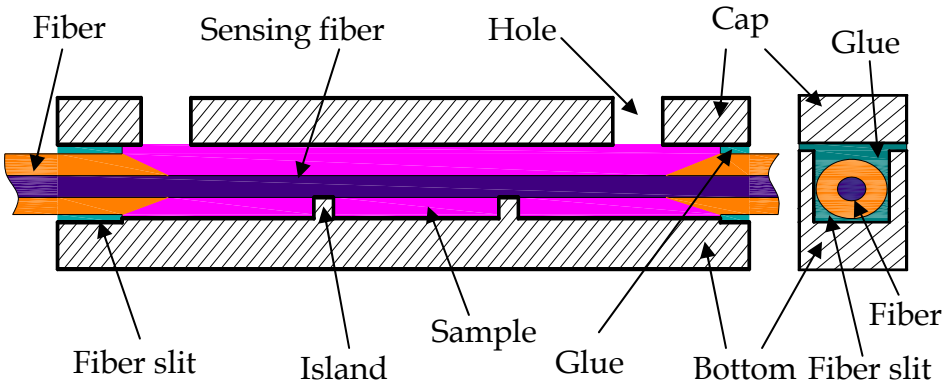

Fig. 8. The schematic structure of the sample cell

The fiber cladding is removed using wet etching, the corrosion solution consists of HF, de-ionized water and CH_3COOH. The function of HF is to etch silica with the well-known reactions:

$$\begin{aligned} 4HF+SiO_2 &\rightarrow SiF_4+2H_2O \\ 6HF+SiO_2 &\rightarrow H_2SiF_6+2H_2O \end{aligned} \tag{24}$$

By adding CH_3COOH as a buffer, the etching process becomes much more gently and the quality of the core surface would be improved greatly.

The velocity of etching is mainly influenced by the parameters list as follows:

1. the concentration of HF. The higher the concentration of the HF in the corrosion solution, the more F^- reacts with silica, the higher the speed of the etching is;
2. the microstructure of silica. Because the silica used in cladding and core is doped with different elements, the microstructures of them are inconsistent, thus the etching speeds of them are different. A compact structure of silica indicates a low etching speed.
3. the temperature. The chemical reaction equations shown in Eq.(24) are endothermic reactions. When the temperature is high, the reaction between HF and the silica is exquisite and the etching speed is high.

As the reaction goes on, the concentration of F^- in the corrosion solution decreases gradually, and the etching speed slows down. However, the radius of the fiber becomes small, which indicates the area-volume ratio of the fiber becomes bigger. In this case, the speed of the etching will increase. So it's really difficult to control the speed of the etching speed carefully. Here, two methods to monitor the fiber's radius are proposed.

1. by monitoring the output power of the fibers. As shown in Fig.9, a powermeter is used to monitor the transmitted power which is a function of the core diameter. Fig.10 shows the relationship between the output power and the etching time. The output power decreases slightly as the cladding is etched by the HF. When the cladding is eaten up and the core is etched by the etching solution, the strength of the output power decreases dramatically. When the core is eaten up, nothing is left in the sample cell, the relative strength of the output power keeps constant, which is the strength of the background noise. The volume ration among HF, de-ionized water, CH_3COOH in the corrosion solution used here is 1.3∶1∶1. According to the relative strength of the output power the radii of the fibers can be estimated accurately.
2. based on the experimental experience. According to the experimental experience, the etching speeds of corrosion solutions of different proportions can be approximately estimated. First, using corrosion solutions with plentiful HF to etch the cladding. When cladding is to be eaten up, solutions with little HF should be chosen to reduce the etching speed and improve the quality of the sensing fibers' surface. During this process, the radius of the fiber should be checked using microscope frequently. When appropriate radius is obtained, the etching process is terminated. In room temperature, as the volume ratio among HF, de-ionized water, CH_3COOH in the solution is 1∶1∶1, the etching speed of the cladding is 20μm per hour, and 30μm per hour of the core.

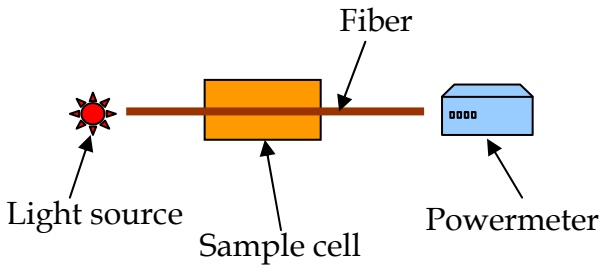

Fig. 9. Experimental set-up of the etching process

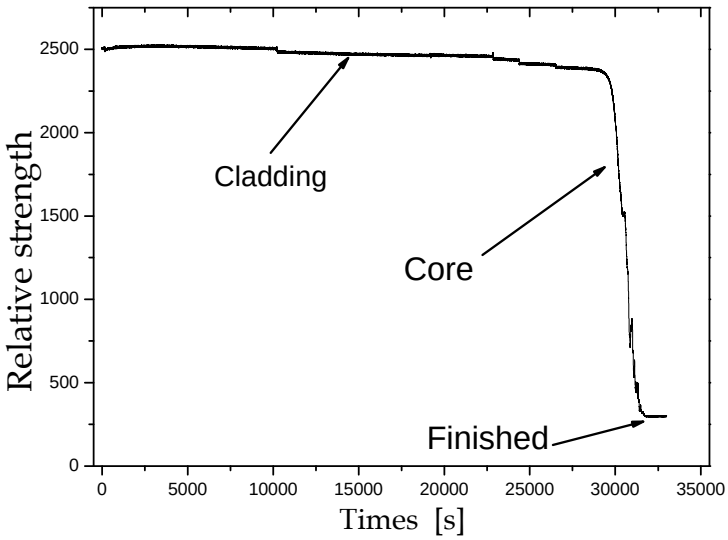

Fig. 10. The relationship between the output power and the etching time

Fig. 11 is the sensing fiber fabricated using the method described above. A cone is obviously observed in the end of the sensing fiber. As shown in Fig.12, when HF erodes the fiber towards the core along the radial direction, cauterization occurs in the fibers' axial direction simultaneously. This is the main reason why the sensing fibers' end is tapered.

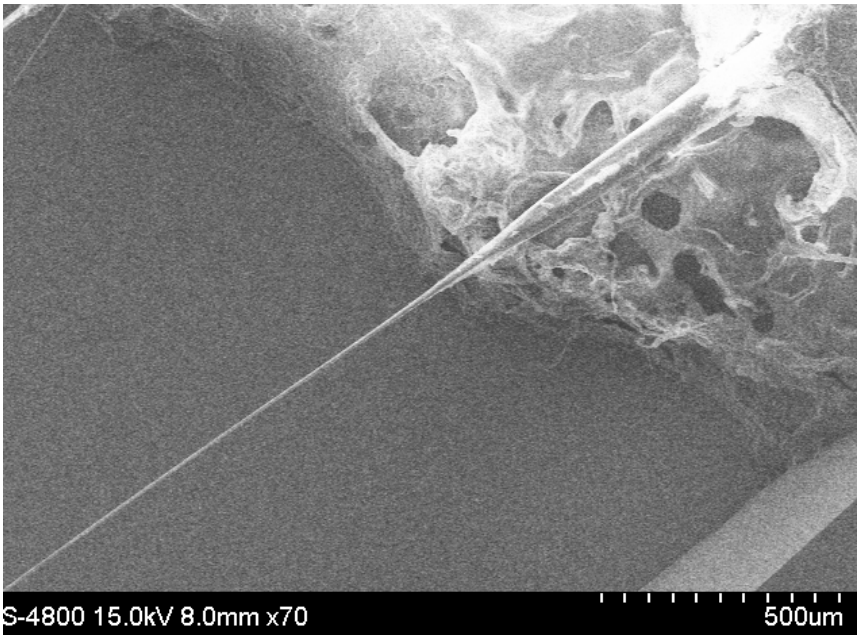

Fig. 11. SEM of the sensing fiber

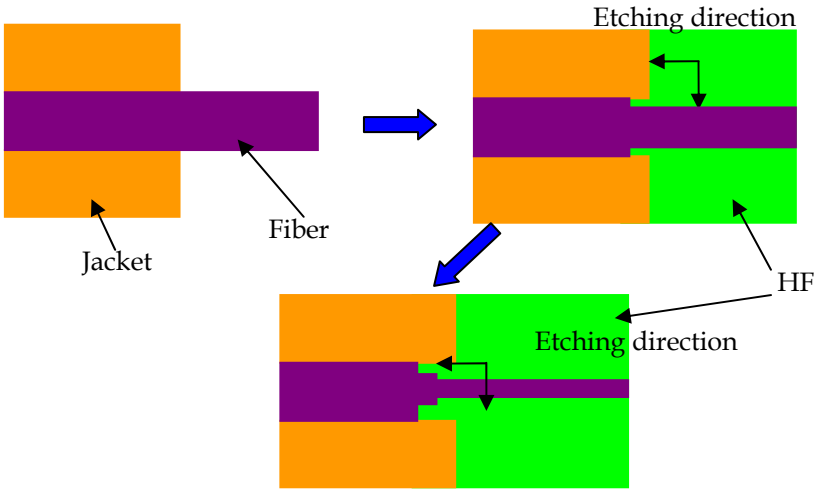

Fig. 12. Schematic of the etching directions of the HF

When the etching terminated, the core of the fiber is washed by de-ionized water and baked to release the remaining liquid. Then the sample cell with the sensing fiber can be used as an optical fiber evanescent field sensor directly, as shown in Fig. 13.

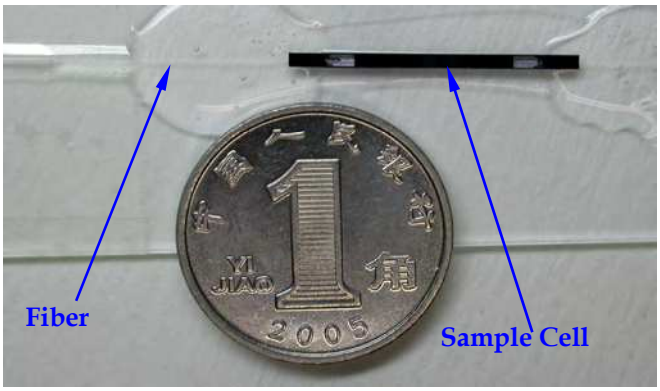

Fig. 13. The optical fiber evanescent field sensor used in the experiments

3.2 Experimental set-up

The experimental set-up is shown in Fig.14. The optics source used here is He-Ne laser (Type 260A，632.8nm). Its minimum output power is 1.8 mW, the maximum drift of it is ±3%, the beam diameter is 2mm and the beam divergence is 1.5 mrad. As shown in Fig.14, the laser is focused and collimated using a couple of lens, then the light is injected into the fiber and the output power is measured by a spectrometer. After the spectrum is analyzed using a computer, the information of the analytes' concentrations is obtained. After the detection, the sensing fiber is refreshed by de-ionized water bath, and the sensing fiber can be used repeatedly.

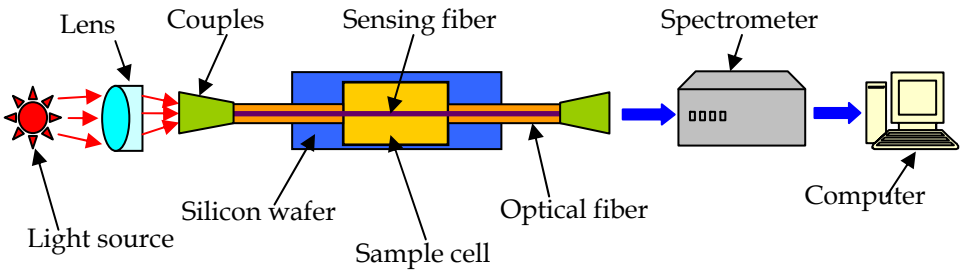

Fig. 14. The experimental set-up

The absorption medium used for experiments is methylene blue (MB) dissolved in de-ionized water and the absorbing peak is 664 nm. Fig.15 is the absorbency spectrum of the methylene blue in visible region. The concentration of the methylene blue used here is 1×10^{-6} mol/L.

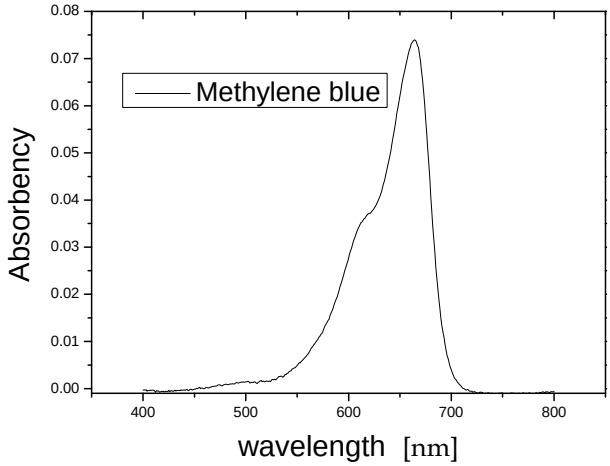

Fig. 15. Absorption spectrum of methylene blue solution in de-ionized water

3.3 Nonlinear relationship between absorbency and the length of the sensing fiber

Fig.16 shows the experimental results of *A*. In the experiments two sensors with different *L*, 7mm and 14mm, are used. The radii of the sensing fibers are both 4μm, and the refractive indexes are both 1.4682. As shown in Fig.16, the ratio of the sensor's absorbency with *L=14mm* to that with *L=7mm* is smaller than two. It shows clearly the sensing efficiency declines as *L* increases. The contribution per unit length of the sensing fiber to *A* drops as *L* increased. When the concentration of MB grows, the ratio increases. This phenomenon is mainly blamed on the sensing fibers' blemish. When the concentration of the analyte is high, the effects of the sensing fibers' disfigurations on *A* become obvious. The most common defects of the sensing fibers are displayed in Fig.17. When constructing optical fiber evanescent field sensors, it is not advised to use long sensing fibers because the sensing efficiency of the sensing fiber per unit length decreases as the sensing fiber becomes long. Also, long sensing fibers are difficult to fabricate and easy to disfigure and break.

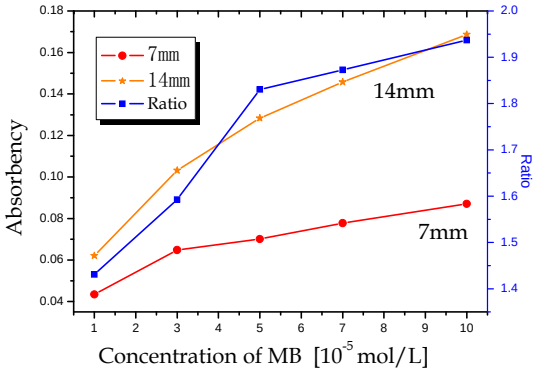

Fig. 16. The experimental absorbency of the sensors with different *L*

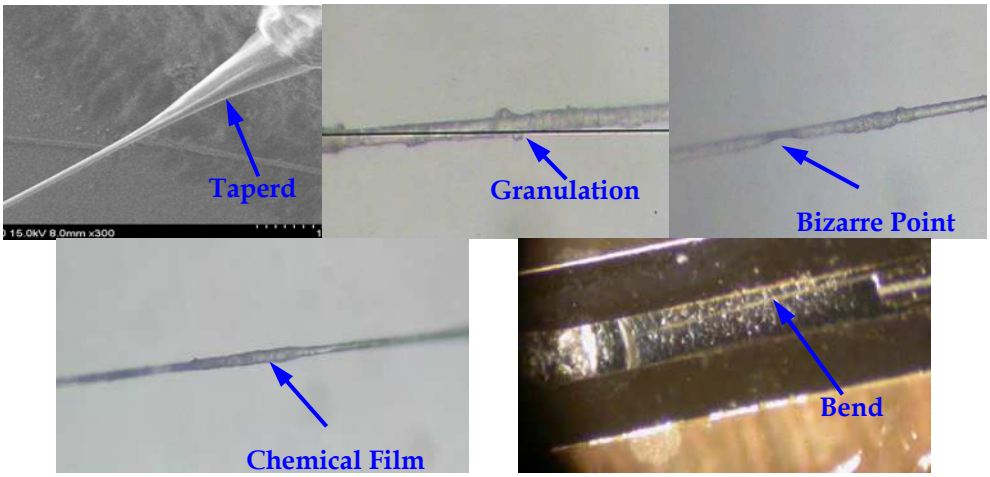

Fig. 17. Defects of the sensing fibers

3.4 The new method to estimate the sensitivity of the sensor

Fig.18a is the picture of the sensor used in the experiments to confirm the accuracy of the novel method proposed here. Fig.18b is the amplificatory image of the sensing fiber. In order to obtain a sensing fiber of high quality and eliminate the deformation caused in the process of encapsulation, the diameter of the sensing fiber used here is 100μm. Sensing fibers with small radii are easy to disfigure and disturb the experimental results. The error of the experimental results can be reduced by using sensing fibers with large radii.

The length of the sensing fiber is 14mm, the refractive index of the fiber core is 1.4577. The wavelength of optic source is 632.8nm. In experiment, the analyte is methylene blue, and its refractive index is adjusted to 1.4550 using glycerol with molar absorption coefficient $27200 L / mol \bullet cm$. The diameter of the sensing fiber is etched to 100μm using hydrofluoric acid.

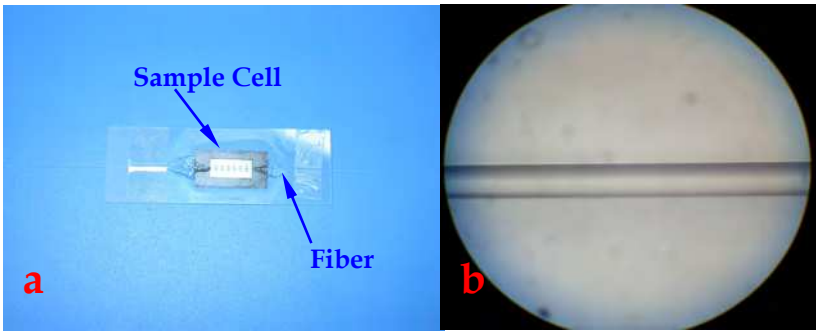

Fig. 18. Sensing fiber used in the experiments

P_{out} / P_{in} against the concentrations of MB obtained from experiments and different calculation schemes are shown in Fig. 19. The curve P represents the method used before. The curves $n = 140$ and $n = 1400$ are the results which obtained using the method proposed here with iterative times 140 and 1400. As shown in Fig.19, the values calculated by our method are much closer to the experimental results, especially when P_{out} / P_{in} is high.

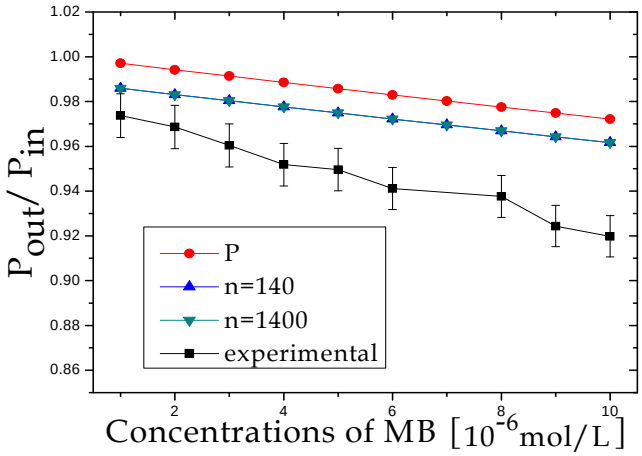

Fig. 19. P_{out} / P_{in} versus the concentrations of MB

From Fig. 20 it is found when $P_{out} / P_{in} > 0.7$ the results obtained using the new method are in a good agreement with the experimental results and more accurate than the results obtained from the methods used before. When the concentration of MB is high, the evanescent field energy absorbed by the analyte is huge. So a small dl should be used to get a more accurate emulational result, which indicates a big n should be chosen, as shown in Fig. 20.

However, when $P_{out} / P_{in} \le 0.7$, a difference between experimental and theoretical values is found. Various reasons have been assigned to this discrepancy. It is mainly caused by the deposition of the methylene blue molecules on the sensing fiber's surface and the disfigurement of the sensing fiber (Ruddy & Maccrait, 1990 ;Potyrailo & Hobbs, 1998; Zhuang et al., 2009b).The effects of the sensing fibers' disfigurements on the results are listed as follow: (1) the surface of the etched core is not perfect and scattering occurs on the interface between the analyte and the sensing fiber, which will decrease the output power of the sensor in experiment; (2) the fiber diameter is unsymmetrical and there are errors in the measurement, which will introduce mistakes to the simulation; (3) the bending loss increases the energy loss in the sensing region, and the values of P_{out} / P_{in} is depressed; (4) when the unclad optical fiber etched, taper will occur in the two ends of the sensing region as described in section 3.1. When light passes through the taper, energy loss happened because of the discontinuity of the modes supported by these two different parts of the fiber and the experimental results will be enhanced (Ahmad & Hench, 2005). As the concentration of MB is high, more molecules will be deposited on the sensing fibers' surface, the absorbency of the sensor will be improved and the discrepancy of the theoretical results from the experimental ones will be enlarged as shown in Fig.20.

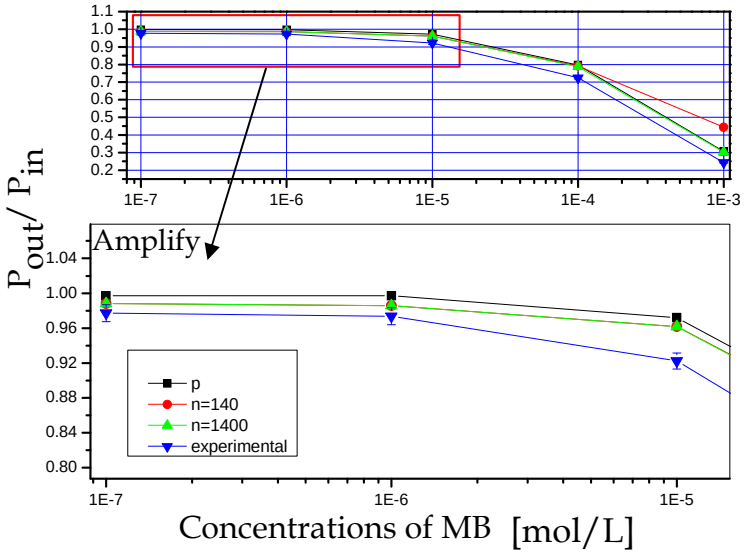

Fig. 20. P_{out} / P_{in} versus the concentrations of MB

4. Conclusion

In this chapter, we have proposed and demonstrated a novel method to estimate the sensitivity of optical fiber evanescent field sensors. In section 1, the importance of constructing mathematical method to estimate the sensitivity of the sensor is described. And the brief introduction of this chapter is also presented in section 1. In section 2, the operation principle of OFEFS is theoretically studied. The effects of the sensing fibers' length, l, on the sensors' absorbency, A, are analyzed. The nonlinear relationship between A and l is also explained in section 2.2. It is found that the contribution per unit length of the sensing fiber to A decreases as l grows. So it does not suggest using long sensing fibers to construct OFEFS. The new method to estimate the sensitivity of OFEFS is proposed in section 2.3. The operation principle of OFEFS is embodied significantly by the mathematical model of the method.

In section 3, the experimental set-up of the sensor is built. The fabrication of the sensor with acicular encapsulation is introduced, and the factors which effect the preparation of the sensing fibers are discussed. The nonlinear relationship between A and l is confirmed with experiments. The new method is prove to be in a good agreement with the experimental results and is more accurate than the methods used before. The divergence of the theoretically results from the experimental ones is explained.

The practical importance of this study lies in helping for understanding, design, and construction of optical fiber evanescent field sensors with high sensitivity.

5. Acknowledgements

The authors acknowledge the supports from West Light Foundation of the Chinese Academy of Sciences (A11K011) and National Natural Science Foundation of China

(60978051). The experiments were done in the national key lab of applied optics of China. The authors would like to thank Professor Yihui Wu for her benefited discussions and helps.

6. References

Ahmad M., Hench L. L., (2005). Effect of Taper Geometries and Launch Angle on Evanescent Wave Penetration Depth in Optical Fibers, *Biosensors and Bioelectronics*, Vol.(20), (2005), pp 1312-1319, ISSN0956-5663

Angela, L., Shankar P. M., Mutharasan R., (2007). A Review of Fiber-optic Biosensors. *Sensors and Actuators B: Chemical,* Vol.125, No.2,(2007), pp 688-703,ISSN 0925-4005

Deng X. H., Wu Y. H., Zhou L. Q., Xu M., (2006). Parameters Analysis of Few-modes Optical Fiber Evanescent Absorption Sensor, *SPIE*, Vol.6032, (2006), pp 603208, ISSN 0277-786X

Gloge D., (1971). Weakly Guiding Fibers, *Appied Optics*, Vol.10, No.10, (1971), pp 2252-2258, ISSN 0003-6935

Guo S., Albin S., (2006). Transmission Property and Evanescent Wave Absorption of Cladded Multimode Fiber Tapers, *Opt. Express*, Vol.11, No.3, (2006), pp 215-223, ISSN 2156-7085

Gupta B. D., Singh C. D., (1994). Fiber-optic Evanescent Field Absorption Sensor: A Theoretical Evaluation, *Fiber and Integrated Optics*, Vol.3, No.4, (1994), pp 433-443, ISSN 0146-8030

Maria E. B., Antonio J. R. S., Fuensanta S. R.,Catalina B. O., (2007). Recent Development in Optical Fiber Biosensors. *Sensors*, Vol.6, No.7,(June 2007), pp 797-859, ISSN 1424-8220

Messica A., Greenstein A., Katzir A., (1996). Theory of Fiber-optic, Evanescent-wave Spectroscopy and Sensors, *Appied Optics*, Vol.35, No.13, (1996), pp 2274-2284, ISBN 0003-6935

Payne F. P., Hale Z. M., (1993). Deviation from Beer's Law in Multimode Optical Fibre Evanescent Field Sensors, *International Journal of Optoelectronics,* Vol.8, (1993), pp 743-748, ISSN 0952-5432

Potyrailo R. A., Hobbs S. E., (1998). Near-ultraviolet Evanescent-wave Absorption Sensor Based on A Multimode Optical Fiber, *Anal. Chem.,* Vol.70, No.8, (1998), pp 1639-1645, ISSN 0003-2700

Ruddy V., Maccrait B. D., (1990). Evanescent Wave Absorption Spectroscopy Using Multimode Fibers, *J.Appl.Phys.* Vol.67, No.10, (1990),pp 6070-6074, ISSN 0021-8979

Wolfbeis O. S., (2006). Fiber-optic Chemical Sensors and Biosensor, *Anal. Chem.*, Vol.78, No.12, (2006), pp 3859-3874, ISSN 0003-2700

Wu Y. H., Deng X. H., Li F., Zhuang X. Y., (2007). Less-mode Optic Fiber Evanescent Wave Absorbing Sensor: Parameter Design for High Sensitivity Liquid Detection, *Sens. Actuators B,* Vol.122, (2007), pp 127-133,ISSN 0925-4005

Yu X., Cottendena A., Jones N. B., (2006). A Theoretical Evaluation of Fibre-optic Evanescent Wave Absorption in Spectroscopy and Sensors. *Optics and Lasers in Engineering,* Vol. 44, (2006), pp 93-101, ISBN 0143-8166

Zhuang X. Y., Wu Y. H., Wang S. R., Zhang P., Liu S. Y., (2009a). Research on the Fiber-optic Evanescent Field Sensor Based on Microfabrication and the Effect of Fiber Length on Its Properties, *Acta Physica Sinca*, Vol.58, No.4, (May 2009), pp 2501-2506, ISSN 1000-3290

Zhuang X. Y., (2009b), Study on the Art of Fiber-optic Evanescent Field Sensor with High Sensitivity, (July 2009), PhD paper of Chinese Academy of Sciences, Beijing, China.

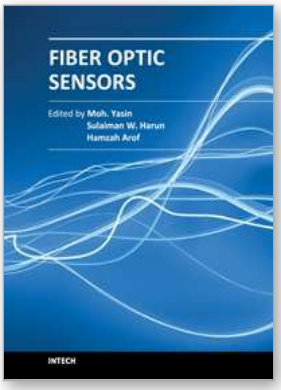

Fiber Optic Sensors

Edited by Dr Moh. Yasin

ISBN 978-953-307-922-6
Hard cover, 518 pages
Publisher InTech
Published online 22, February, 2012
Published in print edition February, 2012

This book presents a comprehensive account of recent advances and researches in fiber optic sensor technology. It consists of 21 chapters encompassing the recent progress in the subject, basic principles of various sensor types, their applications in structural health monitoring and the measurement of various physical, chemical and biological parameters. It also highlights the development of fiber optic sensors, their applications by providing various new methods for sensing and systems, and describing recent developments in fiber Bragg grating, tapered optical fiber, polymer optical fiber, long period fiber grating, reflectometry and interefometry based sensors. Edited by three scientists with a wide knowledge of the field and the community, the book brings together leading academics and practitioners in a comprehensive and incisive treatment of the subject. This is an essential reference for researchers working and teaching in optical fiber sensor technology, and for industrial users who need to be aware of current developments and new areas in optical fiber sensor devices.

INTECH
open science | open minds

InTech Europe
University Campus STeP Ri
Slavka Krautzeka 83/A
51000 Rijeka, Croatia
Phone: +385 (51) 770 447
Fax: +385 (51) 686 166
www.intechopen.com

InTech China
Unit 405, Office Block, Hotel Equatorial Shanghai
No.65, Yan An Road (West), Shanghai, 200040, China
中国上海市延安西路65号上海国际贵都大饭店办公楼405单元
Phone: +86-21-62489820
Fax: +86-21-62489821